Journal of Hyperbolic Differential Equations
Vol. 6, No. 1 (2009) 161–184

World Scientific
www.worldscientific.com

A FULLY PSEUDOSPECTRAL SCHEME FOR SOLVING SINGULAR HYPERBOLIC EQUATIONS ON CONFORMALLY COMPACTIFIED SPACE-TIMES

JÖRG HENNIG* and MARCUS ANSORG†

Max Planck Institute for Gravitational Physics
Am Mühlenberg 1, D-14476 Golm, Germany
**pjh@aei.mpg.de*
†*mans@aei.mpg.de*

Received 14 Jan. 2008
Accepted 4 May 2008

Communicated by H. Friedrich

Abstract. With the example of the spherically symmetric scalar wave equation on Minkowski space-time we demonstrate that a fully pseudospectral scheme (i.e. spectral with respect to both spatial *and* time directions) can be applied for solving hyperbolic equations. The calculations are carried out within the framework of conformally compactified space-times. In our formulation, the equation becomes singular at null infinity and yields regular boundary conditions there. In this manner, it becomes possible to avoid "artificial" conditions at some numerical outer boundary at a finite distance. We obtain highly accurate numerical solutions possessing exponential spectral convergence, a feature known from solving elliptic PDEs with spectral methods. Our investigations are meant as a first step towards the goal of treating time evolution problems in General Relativity with spectral methods in space and time.

Keywords: Wave equation; spectral methods; conformal compactification.

Mathematics Subject Classification 2000: 35L05, 65M70, 83A05

1. Introduction

The simulation of dynamical processes within the theory of General Relativity plays an important role for understanding astrophysical phenomena, for studying the stability of equilibrium configurations by introducing small perturbations and evolving in time and for predicting the properties of the emitted gravitational waves. An ideal way of analyzing such processes carefully would be the construction of explicit solutions to Einstein's field equations. However, due to the mathematical complexity of these equations, even stationary configurations can be described in terms of analytic expressions in only a few exceptional cases. Therefore, the only chance for tackling time dependent processes is the application of numerical methods. Nevertheless, in order to come as close as possible to an explicit solution, it is desirable to find

mathematical descriptions and numerical procedures that permit the computation of a very accurate approximation to the solution in question.

As we demonstrate in this paper, a promising approach towards this goal is the combination of highly accurate (pseudo-) spectral methods with the fruitful concept of conformally compactified space-times.[a] By means of spectral methods, general relativistic equilibrium configurations have been obtained with almost machine accuracy [3]. Dynamical relativistic problems have also been studied utilizing spectral methods (with respect to the spatial directions, combined with finite difference methods in time direction), see e.g. [4]. (For a comprehensive overview of the applications of spectral methods in general relativity, see [10].) However, there is only little experience regarding spectral expansions with respect to space *and* time[b] [13]. As a first step towards the goal of treating time evolution problems in General Relativity with a *fully* pseudospectral scheme, we study model equations, in particular, linear and non-linear wave equations.

The concept of *conformal infinity*, i.e. conformally compactified space-times, was introduced by Penrose [14] in 1964. (For an overview on this topic see [7]; numerical studies can be found in [8, 11, 12, 17].) Within this scheme we are able to carry out the numerical calculations up to infinity. As a consequence, we have no need of numerical outer boundaries at a finite physical distance. At such finite boundaries one usually imposes particular conditions in order to complete the mathematical problem. These conditions have to be compatible with the differential equation to be solved and should lead to a well-posed problem. (Pseudospectral methods are particularly sensitive with respect to this issue. In the worst case, the numerical simulation breaks down after some time when the errors arising due to incompatible boundary conditions accumulate.) However, in any case the physical meaning of such boundary data and their influence to the solution is unclear. That is why we prefer the conformal compactification.

An additional important feature of the conformal approach is the precise determination of gravitational wave signals at null infinity $\mathscr{I}$, which is located at *finite coordinate distance*. Hence, one avoids approximative wave extraction techniques at *finite physical distance*.

Within the conformal concept, hyperbolic differential equations become singular at null infinity. Although it is possible to carry out an appropriate regularization in some special cases (for Einstein's field equations, a suitable reformulation in terms of Friedrich's regular conformal field equations [9] can be used), we demonstrate here that this degeneration of the equations permits a careful numerical treatment. In combination with a fully pseudospectral scheme, we obtain highly accurate numerical solutions (up to 12 or 13 correct digits for a double precision code).

[a]In principle, it is also possible to apply the pseudospectral algorithm described in this paper to arbitrary compact domains if the boundary conditions at $\mathscr{I}$ are replaced by other conditions at the boundaries of these domains.

[b]Only in the context of *finite* and *spectral element methods*, the simultaneous space-time treatment of hyperbolic equations is already more common, see e.g. [15] and references therein.

The paper is organized as follows. In Sec. 2, we recall the conformal compactification of Minkowski space-time. Moreover, we consider the scalar wave equation on this background and derive the boundary conditions to be imposed at the singular points of this equation. The numerical method for solving the singular equation is explained in detail in Sec. 3. In the subsequent section, we give a number of numerical examples in order to test the method and to study the accuracy of the numerical solutions. In Sec. 5, we show that the application of the spectral scheme is not restricted to the homogeneous linear wave equation. To this end we study two additional example equations: an inhomogeneous wave equation and a non-linear wave equation. In Sec. 6, we consider a regularized version of the wave equation and demonstrate that our numerical method is also applicable to this equation. Finally, in Sec. 7, we discuss our results.

2. Wave Equation and Compactification

2.1. *The wave equation*

The model equation to be studied throughout most of this paper is the spherically symmetric wave equation

$$\Box f \equiv f_{,rr} + \frac{2}{r} f_{,r} - f_{,tt} = 0, \quad f = f(r,t) \tag{2.1}$$

on Minkowski space-time with the line element

$$\mathrm{d}s^2 = \mathrm{d}r^2 + r^2(\mathrm{d}\vartheta^2 + \sin^2\vartheta\,\mathrm{d}\varphi^2) - \mathrm{d}t^2 \tag{2.2}$$

using spherical coordinates $(r, \vartheta, \varphi, t)$. The general solution to (2.1),

$$f(r,t) = \frac{a(r+t) + b(r-t)}{r}, \tag{2.3}$$

with $a, b \in C^2(\mathbb{R})$, can be used to investigate the accuracy of the numerical solution. Here we restrict ourselves to solutions which are regular at $r = 0$. As a consequence, we obtain the condition $b(x) = -a(-x)$ for all $x \in \mathbb{R}$, i.e. we consider solutions of the form

$$f(r,t) = \frac{a(t+r) - a(t-r)}{r}. \tag{2.4}$$

For the conformal compactification of Minkowski space-time, one often uses the following coordinate transformation (see [7]):

$$r = \frac{1}{2}\left[\tan(R+T) + \tan(R-T)\right], \quad t = \frac{1}{2}\left[\tan(R+T) - \tan(R-T)\right], \tag{2.5}$$

through which new coordinates R and T are introduced, with $R \in [0, \frac{\pi}{2}]$, $T \in [R - \frac{\pi}{2}, \frac{\pi}{2} - R]$. The line element takes the form

$$\mathrm{d}s^2 = \frac{1}{Q^2 P^2}\left[4(\mathrm{d}R^2 - \mathrm{d}T^2) + \sin^2(2R)(\mathrm{d}\vartheta^2 + \sin^2\vartheta\,\mathrm{d}\varphi^2)\right] \tag{2.6}$$

with

$$Q := \sqrt{2}\cos(R+T), \quad P := \sqrt{2}\cos(R-T). \tag{2.7}$$

Obviously, the metric components are singular at null infinity $\mathscr{I}$, i.e. at $R \pm T = \pi/2$ where $P = 0$ or $Q = 0$. However, the rescaled line element $\mathrm{d}\bar{s}^2 = Q^2P^2\mathrm{d}s^2$ is regular at $\mathscr{I}$. The domain on which R and T are defined is illustrated by the well-known standard conformal diagram, see Fig. 1.

For the wave equation in terms of the coordinates R and T, one obtains

$$QP(f_{,RR} - f_{,TT}) + 2\frac{(Q^2+P^2)f_{,R} + (Q^2-P^2)f_{,T}}{\sin(2R)} = 0. \tag{2.8}$$

The general solution (2.4) can be written as

$$f(R,T) = \frac{A(T+R) - A(T-R)}{\tan(R+T) + \tan(R-T)} \tag{2.9}$$

with $A(x) := a(\tan x)$ for all $x \in [-\pi/2, \pi/2]$. Due to the appearance of the functions P, Q and $\sin(2R)$, the wave equation (2.8) is singular at infinity (as a consequence

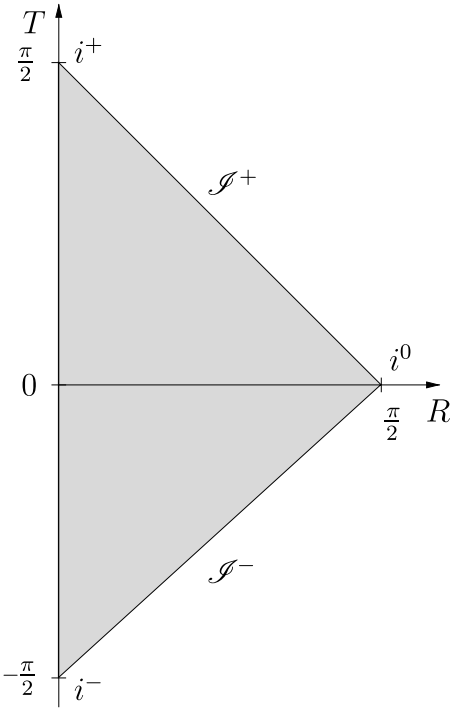

Fig. 1. The standard conformal diagram of Minkowski space-time. The line $R = 0$ corresponds to the center of symmetry $r = 0$. Furthermore, past and future null infinity $\mathscr{I}^{\pm}$, past and future time-like infinity $i^{\pm}$, and space-like infinity i^0 are marked accordingly.

of the compactification) and at the center of symmetry (as an effect of the spherical coordinates), i.e. at the following points:

- i^- and $\mathscr{I}^-$: $R - T = \frac{\pi}{2} \Rightarrow P = 0$
- i^+ and $\mathscr{I}^+$: $R + T = \frac{\pi}{2} \Rightarrow Q = 0$
- i^0: $R \pm T = \frac{\pi}{2} \Rightarrow P = Q = 0$
- $R = 0 : \sin(2R) = 0.$

In the numerical scheme we need to treat these points particularly carefully, in order to derive well-defined boundary conditions, as will be discussed in the next subsection.

We study two different types of initial boundary value problems (IBVP) for the wave equation (2.8), see Fig. 2. In a *hyperboloidal IBVP*, we prescribe initial data (the values of f and the time derivative $f_{,T}$) on the hyperboloidal slice[c] $T = T_{\min}$ and evolve these data up to another hyperboloidal slice $T = T_{\max}$. For the second type we consider a *"standard" Cauchy problem*, in which initial data are given on the particular Cauchy surface $T = t = 0$. From these data, the entire future of f up to i^+ and $\mathscr{I}^+$ is determined. As a consequence of the time symmetry of the wave equation, the past of f can be calculated in the same manner. We thus obtain the function f *everywhere*.

For relativistic time evolution problems, initial data on *Cauchy* surfaces have to be constructed very carefully in order to avoid (logarithmic) singularities at i^0 which cannot be removed easily by means of a coordinate transformation. Solutions to this problem have been discussed by Corvino [5], utilizing a "gluing" technique in order to obtain initial data which are *exact Schwarzschild* data near spatial

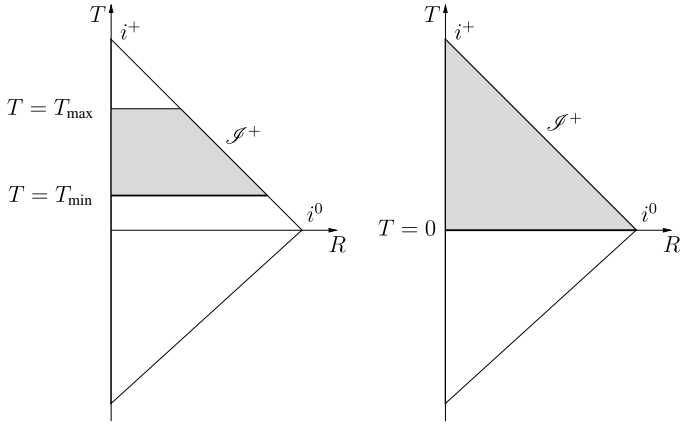

Fig. 2. The numerical domains for the *hyperboloidal initial boundary value problem* (left) and the *standard Cauchy problem* (right).

[c]A slice is called *hyperboloidal* if it is space-like everywhere and extends up to $\mathscr{I}$.

infinity, and more generally by Dain and Friedrich [6]. Note that, on the other hand, there are specific conditions which guarantee the regularity at $\mathscr{I}$ of initial data on *hyperboloidal* slices [1, 2]. For this reason, we concentrate primarily on the hyperboloidal IBVP problem here.

2.2. *Boundary conditions*

The appropriate boundary conditions[d] at the singular boundaries $\mathscr{I}$ and $R = 0$ follow from an analysis of the wave equation (2.8) at these "critical" points. In this investigation, we assume regularity of the solution, i.e. bounded first and second order derivatives.

In order to derive a condition at $R = 0$, we first multiply (2.8) with $\sin(2R)$ and then perform the limit $R \to 0$. Since $P = Q = \cos T$ as $R \to 0$, the following Neumann condition

$$f_{,R} = 0 \tag{2.10}$$

arises. Being a necessary requirement in the context of spherical symmetry, this condition also appears as a consequence of the wave equation.

At $\mathscr{I}^+$ the relation $Q = 0$ holds, and hence the wave equation implies the condition

$$f_{,R} - f_{,T} = 0. \tag{2.11}$$

Similarly, at $\mathscr{I}^-$ one finds that $f_{,R} + f_{,T} = 0$. Thus the tangential derivative of f along $\mathscr{I}$ vanishes, i.e. $f_{,\mu} t^\mu = 0$, where $t^\mu = (1, t^\vartheta, t^\varphi, \mp 1)$ is a tangential vector on $\mathscr{I}$. As a consequence, one may choose either the boundary condition (2.11) at $\mathscr{I}^+$ or the Dirichlet condition

$$f = \text{constant}. \tag{2.12}$$

In the latter case, the constant needs to be read off from the initial data which also extend up to $\mathscr{I}$.

3. Numerical Method

In this section, we describe the numerical procedure for solving the wave equation (2.8) with the boundary conditions (2.10) and (2.11) or (2.12) for the two types of mathematical problems — the hyperboloidal IBVP and the Cauchy problem (see Fig. 2).

[d]Note that we denote any equations to be imposed at inner and outer borders of the numerical domain as "boundary conditions", even if they may be of quite different nature (regularity conditions at coordinate singularities, conditions at $\mathscr{I}$, second order conditions, ...).

The numerical method consists of the following ingredients:

(1) Mapping of the physical domain onto a unit square (or onto several unit squares) by introducing appropriate coordinate transformations. The coordinates being defined on the unit square(s) are referred to as *spectral coordinates*.
(2) Expressing the "wave function" f in terms of another unknown function such that the initial conditions are satisfied automatically.
(3) Expansion of this unknown function in terms of a truncated series of *Chebyshev polynomials* with respect to the spectral coordinates. A particular finite resolution for the numerical approximation is chosen and appropriate grid points in the spectral coordinates on the unit square(s) are identified.
(4) Formulation of an *algebraic system of equations* for the values of the unknown function at the coordinate grid points. This system results from the evaluation of the wave equation and the boundary conditions within the spectral approximation scheme being chosen.
(5) Calculation of the solution of this system by means of the *Newton–Raphson method*.

These points are described in some detail in the following subsections.

3.1. *Spectral coordinates*

Smooth functions can be expressed in terms of spectral Chebyshev expansions provided these functions are defined on an interval or, for more-dimensional functions, on a cross product of intervals. For this reason we introduce an appropriate coordinate mapping through which the physical domain is obtained as the image of the unit square (in the 1+1-dimensional problem considered here).

For the hyperboloidal IBVP, we use the coordinate transformation

$$R = \left[\frac{\pi}{2} - T_{\min} - (T_{\max} - T_{\min})\tau\right]\sigma, \quad T = T_{\min} + (T_{\max} - T_{\min})\tau, \tag{3.1}$$

with $\sigma, \tau \in [0, 1]$. An illustration of these coordinates is given in Fig. 3(a), where particular σ- and τ-coordinate lines are shown. The physical boundaries $T = T_{\min}$, $T = T_{\max}$, $R = 0$ and $\mathscr{I}^+$ are mapped to the edges $\tau = 0$, $\tau = 1$, $\sigma = 0$ and $\sigma = 1$ of the square, respectively.

Note that at the points i^0 and i^+ the wave function is not analytic with respect to the coordinates R and T. Therefore, in the case of the standard Cauchy problem, it is necessary to introduce a singular coordinate mapping through which the wave function becomes analytic with respect to the spectral coordinates. To this end we divide up the physical domain into two triangular subdomains and map each of these subdomains onto a unit square, see Fig. 3(b). We use the particular coordinates

$$R = \frac{\pi}{4}\left[2\sigma + (1-\sigma)\tau\right], \quad T = \frac{\pi}{4}(1-\sigma)\tau \tag{3.2}$$

in domain 1 and

$$R = \frac{\pi}{4}(1-\sigma)\tau, \quad T = \frac{\pi}{4}\left[2\sigma + (1-\sigma)\tau\right] \tag{3.3}$$

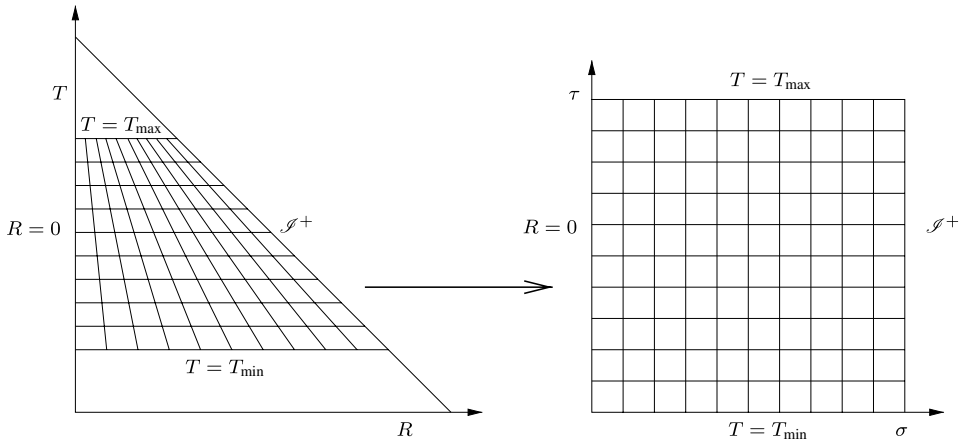

(a) Spectral coordinates — Hyperboloidal initial value problem

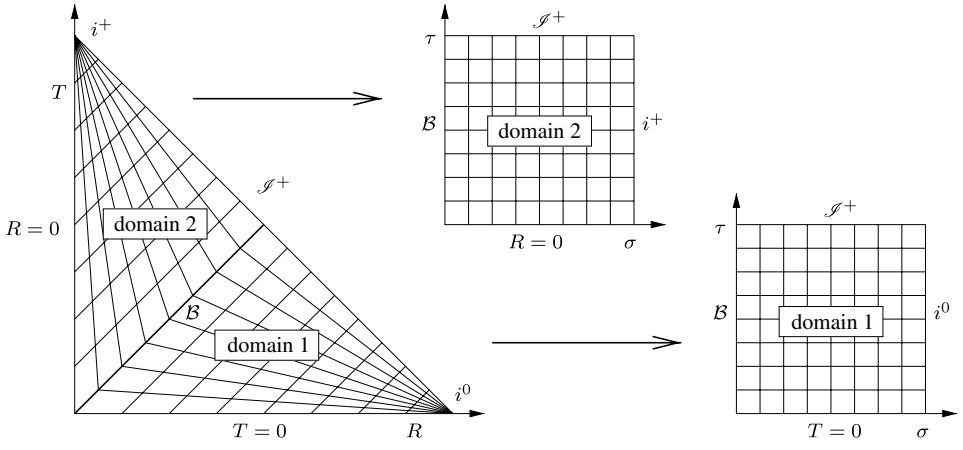

(b) Spectral coordinates — Cauchy problem

Fig. 3. Illustration of the spectral coordinates σ and τ for the two types of IBVPs.

in domain 2. The edges of the two squares correspond to $R = 0$, $T = 0$, i^0, i^+, sections of $\mathscr{I}^+$, and, additionally, the common boundary $\mathcal{B} = \{(R, T) : R = T; 0 \leq R \leq \pi/4\}$ between the two domains. Boundary conditions at $\mathcal{B}$ can be derived from the requirement that the wave function f be analytic in a neighborhood of the initial slice $T = 0$. As a consequence of the wave equation, f is then analytic everywhere in the domain of dependence. In particular, for the standard Cauchy problem it follows that f possesses a continuous and differentiable transition at $\mathcal{B}$.

The particular choice of the spectral coordinates is not unique. Also the boundary $\mathcal{B}$ (in the Cauchy problem) could have been chosen to be at a different location (e.g. at $T = \alpha R$ with $\alpha = \text{constant} \neq 1$). Although our choice ($T = R$) represents

a *characteristic* curve of the wave equation, in general the curve does not need to possess specific features with respect to the underlying equation.

3.2. *Initial conditions*

A prescribed set of initial conditions for the wave equation, to be imposed at $T = T_{\min}$ (i.e. at $\tau = 0$), can be satisfied automatically through a specific ansatz for the wave function f. For given functions $G(R)$ and $H(R)$ with

$$f(R, T = T_{\min}) = G(R), \quad f_{,T}(R, T = T_{\min}) = H(R), \tag{3.4}$$

we replace f, expressed as a function of the spectral coordinates σ and τ, by a function f_2 via

$$f(\sigma, \tau) = f_0(\sigma) + f_1(\sigma)\tau + f_2(\sigma, \tau)\tau^2. \tag{3.5}$$

The functions $f_0(\sigma)$ and $f_1(\sigma)$ are given in terms of the initial data by

$$f_0(\sigma) = f(\sigma, \tau = 0) = G[R(\sigma, \tau = 0)] \tag{3.6}$$

and

$$f_1(\sigma) = \left.\frac{\partial f(\sigma, \tau)}{\partial \tau}\right|_{\tau=0} = \left.\frac{\partial f}{\partial R}\frac{\partial R}{\partial \tau} + \frac{\partial f}{\partial T}\frac{\partial T}{\partial \tau}\right|_{\tau=0} = \left.\frac{\partial G}{\partial R}\frac{\partial R}{\partial \tau} + H\frac{\partial T}{\partial \tau}\right|_{\tau=0}. \tag{3.7}$$

In this manner, for any regular choice of the new unknown quantity $f_2(\sigma, \tau)$, the function $f(\sigma, \tau)$ as given in (3.5) satisfies the correct initial conditions at $\tau = 0$.

3.3. *Chebyshev approximation*

In a spectral method, the unknown functions are approximated in terms of appropriate basis functions. Here we choose *Chebyshev polynomials* defined on the interval $[0, 1]$. In particular, we approximate f_2 by

$$f_2(\sigma, \tau) \approx \sum_{i=0}^{N_\sigma} \sum_{j=0}^{N_\tau} c_{ij} T_i(2\sigma - 1) T_j(2\tau - 1), \tag{3.8}$$

where T_n denotes the nth Chebyshev polynomial, c_{ij} the *Chebyshev coefficients*, and

$$n_\sigma = N_\sigma + 1, \quad n_\tau = N_\tau + 1 \tag{3.9}$$

are the prescribed resolution orders with respect to the spectral directions.

In accordance with this choice we introduce the following spectral *collocation points* $P_{ij} = (\sigma_i, \tau_j)$ at which the the wave equation and the boundary conditions are

evaluated in order to build up an algebraic system of equations (see next subsection):

$$\sigma_i = \sin^2\left(\frac{\pi}{2}\frac{i}{N_\sigma}\right), \quad i = 0, 1, \ldots, N_\sigma, \tag{3.10}$$

$$\tau_j = \sin^2\left(\frac{\pi}{2}\frac{j}{N_\tau}\right), \quad j = 0, 1, \ldots, N_\tau. \tag{3.11}$$

Note that we choose to use the extrema of the Chebyshev polynomials (Gauss–Lobatto collocation points) so as to have gridpoints lying on the boundaries.

3.4. *Algebraic system of equations*

For a given spectral approximation order, it is straightforward to compute from the values $X_{ij} := f_2(\sigma_i, \tau_j)$

(1) the Chebyshev coefficients of f_2;
(2) the Chebyshev coefficients of the first and second derivatives of f_2 with respect to the spectral coordinates σ and τ;
(3) the values of these derivatives at the spectral collocation points $P_{ij} = (\sigma_i, \tau_j)$.

For any values X_{ij} it thus becomes possible to "evaluate" the wave equation at the spectral gridpoints by inserting the function and derivative values. The mathematical task to be solved can therefore be formulated as follows: *calculate the $n_\sigma \times n_\tau$ unknown values X_{ij} as the solution of the algebraic system of the $n_\sigma \times n_\tau$ equations $F_{ij}(X_{kl}) = 0$, where F_{ij} is the left-hand side of the wave equation or boundary condition evaluated from X_{kl} at the grid-point (i, j).*

In the case of the hyperboloidal IBVP the following equations arise:

$$\begin{gathered}\text{at } R = 0 : f_{,R} = 0, \quad \text{at } \mathscr{I}^+ : f_{,R} - f_{,T} = 0, \\ \text{otherwise: the wave equation,}\end{gathered} \tag{3.12}$$

and in the Cauchy problem

$$\begin{gathered}\text{at } R = 0 : f_{,R} = 0, \quad \text{at } \mathscr{I}^+, \, i_0 \text{ and } i^+ : f = 0, \\ \text{at } \mathcal{B}\text{: } f \text{ and } \frac{\partial f}{\partial n} \text{ continuous}, \quad \text{otherwise: the wave equation,}\end{gathered} \tag{3.13}$$

where $\partial f/\partial n$ denotes the normal derivative with respect to the boundary $\mathcal{B}$ (here, $\partial f/\partial n \propto f_{,R} - f_{,T}$). The condition $f = 0$ at infinity is true for all initial data vanishing at infinity. ($f = 0$ at infinity is automatically guaranteed for all bounded functions $A(x)$ in the general solution (2.9) of the wave equation.)

It turns out that there are two exceptional points at which the conditions (3.12) or (3.13) are already satisfied as a consequence of the "ansatz" (3.5):

$$\text{Point 1:} \quad \sigma = \tau = 0, \qquad \text{Point 2:} \quad \sigma = 1, \tau = 0.$$

These points correspond to the intersections of the initial slice $T = T_{\min}$ with $R = 0$ and with $\mathscr{I}^+$ (in the hyperboloidal IBVP) or with i^0 (in domain 1 in the Cauchy

problem). For example, at $\sigma = \tau = 0$, the condition $f_{,R} = 0$ reduces to $g_{,R} = 0$ which is already satisfied for the spherically symmetric initial data.

Therefore, additional conditions need to be imposed at these two points, in order to complete the algebraic system of equations. As with the various other boundary conditions, these conditions also follow from the wave equation (2.8).

In the limit $R \to 0$, one obtains

$$3f_{,RR} - f_{,TT} - 4\tan T\, f_{,T} = 0. \tag{3.14}$$

At $\mathscr{I}^+$ the following condition can be derived

$$f_{,RR} + f_{,TT} - 2f_{,RT} = 0. \tag{3.15}$$

Finally, in the case of the Cauchy problem, at $\sigma = 1$ and $\tau = 0$, we impose the condition

$$f_2 = 0. \tag{3.16}$$

This is a consequence of (3.5) and the fact that $f = 0$ at $\mathscr{I}$. Since $f_0 = f_1 = 0$ for $\sigma = 1$, it follows that $f_2(\sigma = 1, \tau \neq 0) = 0$. Hence, for a continuous function, $f_2(\sigma = 1, \tau = 0) = 0$ holds.

3.5. *Newton Raphson method*

Throughout most of this paper, we concentrate on the linear wave equation, for which the system $F_{ij}(X_{kl}) = 0$ is linear. A corresponding solution method as e.g. the Gauss–Jordan elimination or the LU decomposition would provide us with the solution to our IBVP. However, in order to tackle non-linear equations it is necessary to use a more general scheme. For this reason we choose the Newton Raphson method.

We define the $n_\sigma \times n_\tau$-dimensional vectors

$$\mathbf{X} := (X_{00}, X_{01}, \ldots, X_{0N_\tau}, X_{10}, \ldots, X_{1N_\tau}, \ldots, X_{N_\sigma 0}, \ldots, X_{N_\sigma N_\tau}), \tag{3.17}$$

$$\mathbf{F} := (F_{00}, F_{01}, \ldots, F_{0\,N_\tau}, F_{10}, \ldots, F_{1N_\tau}, \ldots, F_{N_\sigma\, 0}, \ldots, F_{N_\sigma N_\tau}), \tag{3.18}$$

containing all components of X_{ij} and F_{ij}. Hence, the system of equations can be written as

$$\mathbf{F}(\mathbf{X}) = \mathbf{0}. \tag{3.19}$$

Within the Newton Raphson method, the system (3.19) is solved iteratively using an "initial guess" $\mathbf{X}^0$ and computing the successive vectors

$$\mathbf{X}^{n+1} = \mathbf{X}^n - [\mathbf{F}'(\mathbf{X}^n)]^{-1}\mathbf{F}(\mathbf{X}^n). \tag{3.20}$$

Here, we approximate the *Jacobi matrix* $\mathbf{F}' = (\partial F_i/\partial X_j)$ through a second order finite difference representation and obtain the inverse via an LU decomposition.[e]

[e]Note that for our 1+1-dimensional IBVP a direct matrix inversion is computationally feasible. However, for higher-dimensional problems such methods are too computationally expensive and one requires the use of iterative matrix inversion methods.

4. Test of the Method with Explicit Examples

4.1. *Numerical accuracy*

We study several explicit examples in order to investigate the effectiveness of our numerical method. From (2.9), we can construct a particular solution to the wave equation by choosing the appropriate function $A(x)$. For a given time interval $[T_{\min}, T_{\max}]$, where $0 \leq T_{\min} < T_{\max} \leq \frac{\pi}{2}$ (equal signs in the case of the standard Cauchy problem), we read off f and $f_{,T}$ at $T = T_{\min}$ as initial data for the numerical method and solve for f in the entire domain expanding up to the maximal time $T = T_{\max}$.

As a measure of the overall numerical accuracy, we calculate the *numerical residual*

$$R_{\text{num}}(n_\sigma, n_\tau) := \max_{(\sigma,\tau)\in[0,1]^2} |f_{\text{num}}(\sigma,\tau) - f_{\text{an}}(\sigma,\tau)|\,, \tag{4.1}$$

where f_{num} and f_{an} denote the numerical and analytical solution, respectively.

In order to investigate to what extent the numerical method is effective and leads to accurate solutions, we compare R_{num} to the *analytical* error caused by an exact Chebyshev representation of the given resolution order. This error is given by the following *analytical residual*

$$R_{\text{an}}(n_\sigma, n_\tau) := \max_{(\sigma,\tau)\in[0,1]^2} |f_{\text{approx}}(\sigma,\tau) - f_{\text{an}}(\sigma,\tau)| \tag{4.2}$$

and describes the maximal difference between the analytical solution f_{an} and its Chebyshev approximation

$$f_{\text{approx}} = \sum_{i=0}^{n_\sigma-1} \sum_{j=0}^{n_\tau-1} \tilde{c}_{ij} T_i(2\sigma-1) T_j(2\tau-1) \tag{4.3}$$

of the order (n_σ, n_τ).[f]

Since the error (4.2) of the Chebyshev approximation (4.3) is close to the smallest possible polynomial approximation error (which one would obtain for the *optimal* approximation polynom of the particular function to be approximated), R_{an} provides a good measure for the effectiveness and potential accuracy of our numerical method. In the subsequent subsection, we display plots of both residuals R_{num} and R_{an} for several example solutions.

A well-known property of Chebyshev approximations for smooth functions is an exponential decay of R_{an} with increasing resolution (up to a final saturation level of order 10^{-14} or 10^{-15} due to the finite machine accuracy of 16 numerical digits being used). As will be demonstrated below, the numerical residuals R_{num} also possess an exponential fall-off and reach a final saturation level near the final level of R_{an}.

Another important issue is the dependence of the numerical residual on the size of the time interval $[T_{\min}, T_{\max}]$. It turns out that without substantial loss of

[f]For the calculation of the coefficients $\tilde{c}_{ij}$ we have used the *exact* values of the function f_{an} at the gridpoints (σ_i, τ_j).

accuracy we may choose a time step that is comparable to or larger than a spatial scale implied by the initial data.

4.2. *Numerical examples*

As a first example, we consider $A(x) = x$ in Eq. (2.9), i.e. the analytical solution

$$f(R,T) = \frac{2R}{\tan(R+T) + \tan(R-T)}. \tag{4.4}$$

(A plot of this solution can be found in Fig. 9 in Appendix A.) The numerical and analytical residuals (as defined in (4.1), (4.2)) for a small and a large time interval in the hyperboloidal IBVP are shown in Fig. 4. We have chosen the resolutions n_σ and n_τ to be connected by $n_\sigma = 2n_\tau$.

As expected, R_{an} exhibits *geometric convergence* (the graph is roughly a straight line in the logarithmic plot). For $n_\tau = 18$, a saturation level is reached at a value below 10^{-14}. The numerical residual R_{num} shows the same qualitative behavior: it decreases almost linearly in the logarithmic plot until it reaches a saturation level at a value of about 10^{-12} for $n_\tau = 17$ in the case of the small time interval and also at almost 10^{-12} for $n_\tau = 20$ in the case of the large time interval. Thus, approximately the same accuracy of about 12 correct digits can be obtained for both the small and the large time interval.

We study the solution in question with $A(x) = x$ also as a standard Cauchy problem. The numerical result is presented in Fig. 5. The final saturation level of about 10^{-13} (which is reached for 20×20 collocation points in each numerical domain) is even below the final level in the hyperboloidal problem. The reason for this might be the particular treatment of the points i^0 and i^+, see Sec. 3.1.

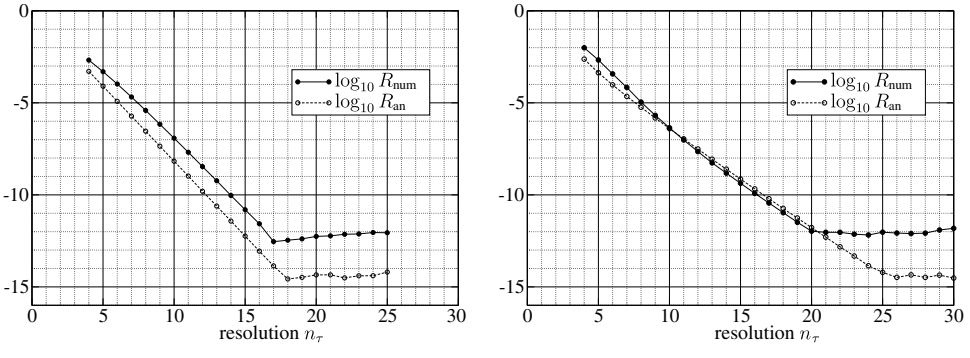

Fig. 4. Plot of the numerical and analytical residuals for the example solution with $A(x) = x$. Parameters: $n_\sigma = 2n_\tau$, $T_{\min} = 0.3$. Left panel: $T_{\max} = 0.6$. Right panel: $T_{\max} = 1.2$. (Note that with the latter value of $T_{\max}$ a fairly large time interval is realized since future time-like infinity is characterized by $T = \pi/2 = 1.57\ldots$.)

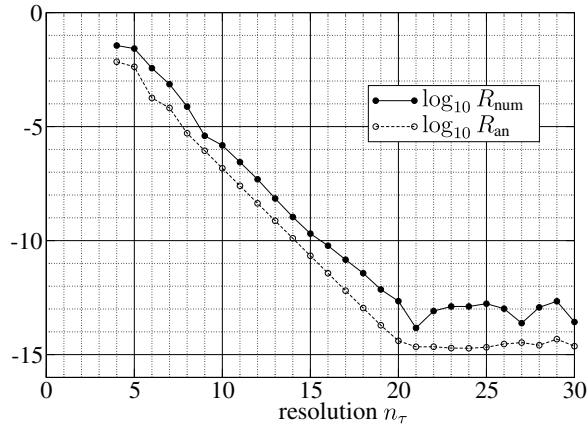

Fig. 5. Numerical accuracy in the standard Cauchy problem with $A(x) = x$. The numerical resolutions are chosen to be related by $n_\sigma = n_\tau$ in both subdomains.

Table 1. List of the further numerical examples for the hyperboloidal IBVP, see Figs. 6 and 12.

	$A(x)$	Remark	$T_{\min}$	$T_{\max}$	n_σ
(A)	$\frac{1}{b}\sin(bx)$ with $b = 10$	arbitrary number of minima and maxima depending on b	0.3	0.6	$2n_\tau$
(B)	$\frac{1}{b}\sin(bx)$ with $b = 20$	cf. (A)	0.3	0.6	$2n_\tau$
(C)	$(x - T_{\min})^2(x - T_{\min} + 1)$	incoming "hill"	0.3	1.2	$2n_\tau$
(D)	$\mathrm{e}^{-64(x-0.7)^2}$	incoming Gauss-like pulse, reflected at $R = 0$, outgoing with inversed amplitude	0.3	1.0	$2n_\tau$
(E)	$\mathrm{e}^{-64(x-1.1)^2} - \mathrm{e}^{-64(x+0.1)^2}$	two Gauss-like pulses crossing each other	0.3	0.9	$2n_\tau$
(F)	$-30\mathrm{e}^{-\frac{1}{(x+0.8)(0.2-x)}}$ (if $-0.8 < x < 0.2$, otherwise $A(x) = 0$)	outgoing pulse with compact support (C^∞, not analytic)	0.3	0.6	$4n_\tau$

A number of further numerical examples for the hyperboloidal IBVP are summarized in Table 1. (For plots of these solutions see Fig. 12 in Appendix A.) The corresponding plots of the numerical accuracies are shown in Fig. 6. In these examples, a saturation level between 10^{-10} and 10^{-13} is reached for sufficiently large spectral resolutions. An exception is example F, which describes an initial pulse on a compact support. Even with a resolution of $n_\sigma = 160$, $n_\tau = 40$ (where the saturation level is not yet reached) the numerical solution is correct only in the first 8 digits. This follows from the fact that a very accurate spectral approximation of a non-analytic C^∞-function requires high resolution. As a consequence, the numerical techniques become expensive.

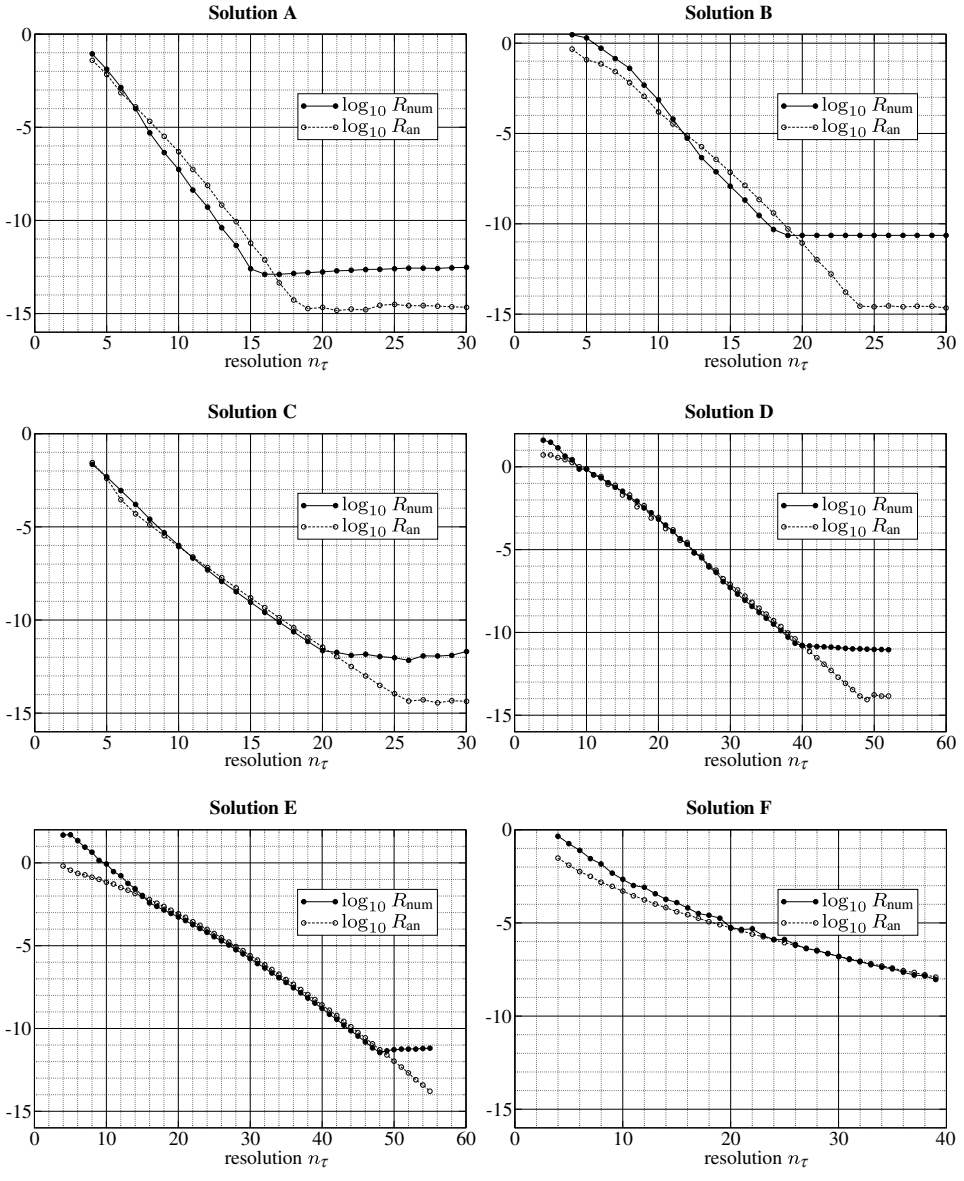

Fig. 6. The residuals of the examples for the hyperboloidal IBVP in Table 1, see Fig. 12.

5. Other Equations

The numerical examples presented in the previous section provide evidence for the fact that highly accurate solutions to the wave equation can be obtained using a fully pseudospectral scheme. In this section, we demonstrate that the method also works in the case of other differential equations. We discuss two particular

modifications of the wave equation: an inhomogeneous wave equation and a nonlinear wave equation.

5.1. *Inhomogeneous wave equation*

An interesting feature of time evolution problems in General Relativity is the possible formation of singularities from completely regular initial data, e.g. the scenario of the formation of a black hole from a collapsing star. For this reason we investigate the applicability of our numerical method to an example solution which develops a pole like singularity. In particular we study how closely to this critical point the numerical domain can be located. Since solutions to the homogeneous linear wave equation do not develop singularities from regular initial data, we consider a particular *inhomogeneous* linear wave equation,

$$QP(f_{,RR} - f_{,TT}) + 2\frac{(Q^2+P^2)f_{,R} + (Q^2-P^2)f_{,T}}{\sin(2R)} = I(R,T), \tag{5.1}$$

where the right-hand side $I(R,T)$ is taken such that f develops a pole after a finite time. This property is guaranteed by choosing the solution

$$f(R,T) = \frac{1}{(R^2-R_0^2)^2 + (T^2-T_0^2)^2}, \tag{5.2}$$

which is singular for $R = R_0$, $T = T_0$. From this expression, we can calculate the corresponding inhomogeneity I as well as the initial data. Equation (5.1) can be solved in the same manner as the homogeneous wave equation. Note that the boundary conditions at $\mathscr{I}^+$ and at the "exeptional points", cf. Sec. 3.4, take on a different form. At $\mathscr{I}^+$, instead of (2.11), we impose the condition

$$4\sin(2R)(f_{,R} - f_{,T}) = I. \tag{5.3}$$

For $\sigma = \tau = 0$, we rewrite (3.14) accordingly:

$$3f_{,RR} - f_{,TT} - 4\tan T f_{,T} = \frac{I}{2\cos^2 T}. \tag{5.4}$$

Finally, at $\sigma = 1$, $\tau = 0$, we replace (3.15) by the condition

$$2\sin(2R)(f_{,RR} + f_{,TT} - 2f_{,RT}) = I_{,R}. \tag{5.5}$$

The residuals for the numerical solution of the hyperboloidal IBVP with the exact solution (5.2) are shown in Fig. 7. In Fig. 7(a)–(c), the solution is calculated in a hyperboloidal domain with a fixed value of $T_{\min} = 0.3$ and increasing maximal time values $T_{\max}$ approaching the singularity. One observes that more and more resolution with respect to the time direction is required in order to reach the saturation level. Furthermore, the maximal accuracy obtained decreases slightly. However, even in a small vicinity of the pole, the solutions are very accurate for a sufficiently large resolution.

In Fig. 7(d), the inhomogeneous wave equation is solved within a narrow hyperboloidal strip with $T_{\min} = 1.1$ and $T_{\max} = 1.2$. Although the singularity (located

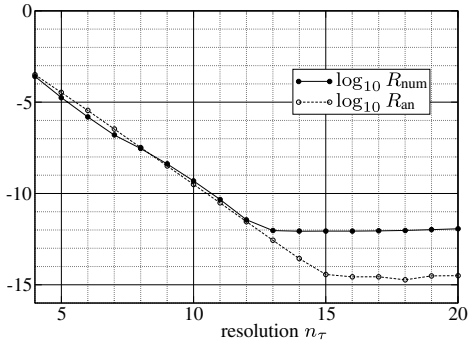

(a) Parameters: $T_{\min} = 0.3,\ T_{\max} = 0.6,$ $n_\sigma = 2n_r$

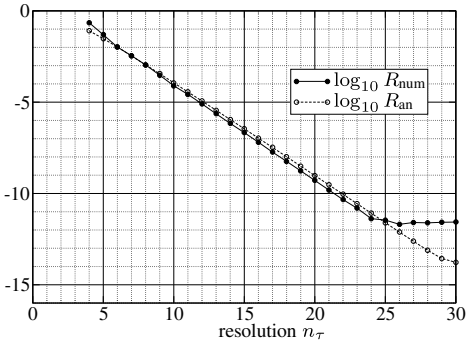

(b) Parameters: $T_{\min} = 0.3,\ T_{\max} = 1.0,$ $n_\sigma = 2n_r$

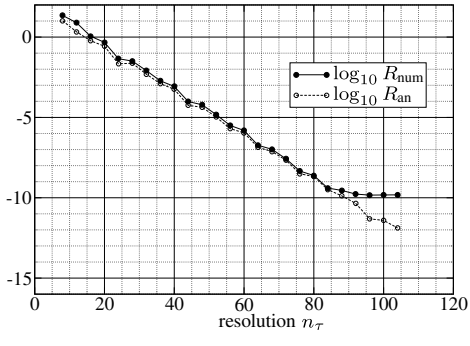

(c) Parameters: $T_{\min} = 0.3,\ T_{\max} = 1.25,$ $n_\sigma = n_r/4$

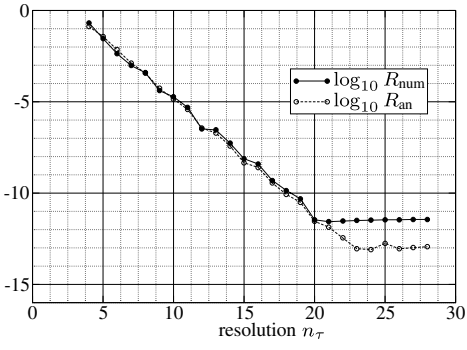

(d) Parameters: $T_{\min} = 1.1,\ T_{\max} = 1.2,$ $n_\sigma = n_r$

Fig. 7. The residuals $R_{\rm num}$ and $R_{\rm an}$ for solutions of the inhomogeneous wave equation, being calculated on different time intervals $[T_{\min}, T_{\max}]$. The pole is located at $R_0 = 0.1$, $T_0 = 1.3$. A plot of the solution is shown in Fig. 10 in Appendix A.

at $R_0 = 0.1$, $T_0 = 1.3$) is close to this domain, the solution is highly accurate (11 correct digits) and the numerical saturation is reached for a moderate value of $n_\tau = 20$.

The above examples demonstrate the applicability of our fully spectral method to solutions which encounter a singular behavior. The numerical solutions being obtained retain high accuracy, provided that an appropriate resolution is chosen.

5.2. *Non-linear wave equation*

In the preceding sections, we have studied *linear* differential equations. However, in view of future applications in General Relativity, it is interesting to apply our numerical method to *non-linear* equations. (In an appropriate formulation, the Einstein equations reduce to a set of non-linear wave equations.)

To this end, we consider the example equation

$$\Box f \equiv f_{,rr} + \frac{2}{r} f_{,r} - f_{,tt} = \lambda \left[r(f_{,r}^2 - f_{,t}^2) + 2 f f_{,r} + \frac{1}{r} f^2 \right] \tag{5.6}$$

with $\lambda = \text{constant}$. The general solution (regular at $r = 0$) is given by[g]

$$f(r,t) = -\frac{1}{\lambda r} \ln \left[1 + \lambda \left(a(t+r) - a(t-r) \right) \right]. \tag{5.7}$$

We introduce again the coordinates R and T [see (2.5)] and obtain the non-linear wave equation

$$\begin{aligned} &QP \left[QP(f_{,RR} - f_{,TT}) + \frac{2}{\sin(2R)} \left[(Q^2 + P^2) f_{,R} + (Q^2 - P^2) f_{,T} \right] \right] \\ &\quad = \lambda \left[\sin(2R) QP (f_{,R}^2 - f_{,T}^2) + 2f \left[(Q^2 + P^2) f_{,R} + (Q^2 - P^2) f_{,T} \right] + 4 \frac{QP}{\sin(2R)} f^2 \right] \end{aligned} \tag{5.8}$$

with Q and P as defined in (2.7). The general solution reads

$$f(R,T) = -\frac{2}{\lambda} \frac{\ln \left[1 + \lambda (A(T+R) - A(T-R)) \right]}{\tan(R+T) + \tan(R-T)}. \tag{5.9}$$

As with the linear wave equation, the boundary conditions can be obtained by analyzing the equation at the singular points. In this manner we find the conditions

$$Q^2 f_{,R} = \lambda f^2 \quad \text{at} \quad R = 0, \quad f_{,R} - f_{,T} = 0 \quad \text{at} \quad \mathscr{I}^+ \tag{5.10}$$

and, additionally, at the "exceptional points" (see Sec. 3.4)

$$3 f_{,RR} - f_{,TT} - 4 \tan T f_{,T} = \frac{4\lambda}{\cos^2 T} f f_{,R} \quad \text{at } \sigma = 0, \tau = 0, \tag{5.11}$$

and

$$f_{,RR} + f_{,TT} - 2 f_{,RT} = 0 \quad \text{at } \sigma = 1, \tau = 0. \tag{5.12}$$

Note that in the limit $\lambda \to 0$ one recovers the boundary conditions of the *linear* wave equation.

As an example, we choose the particular solution (5.9) obtained for $A(x) = x$ (see Fig. 11 in Appendix A). Again, we read off the corresponding initial data and apply our numerical method to solve the IBVP. The results are displayed in Fig. 8.

We have solved the hyperboloidal IBVP for both a small and a large time interval (left and right panel in Fig. 8). One finds a numerical accuracy of about 10 to 11 correct digits. Hence, the solution is nearly as precise as the corresponding example solution of the *linear* wave equation with $A(x) = x$, cf. Fig. 4.

[g]The solution can be obtained by writing f as $f(r,t) = \Phi(r,t)/r$ and introducing null coordinates $u = r + t$, $v = r - t$. Then, Eq. (5.6) reduces to $\Phi_{,uv} = \lambda \Phi_{,u} \Phi_{,v}$, which can be solved easily.

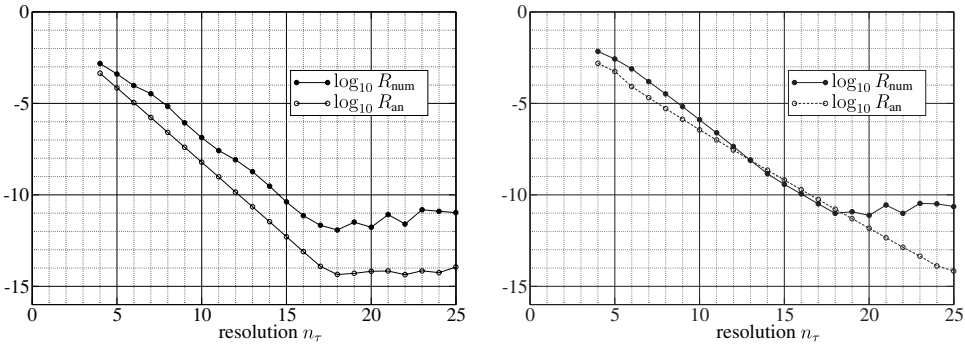

Fig. 8. The numerical and analytical residuals for the example solution to the non-linear wave equation with $A(x) = x$, see (5.9). Parameters: $\lambda = 1$, $n_\sigma = 2n_\tau$, $T_{\min} = 0.3$. Left panel: $T_{\max} = 0.6$. Right panel: $T_{\max} = 1.2$, see Fig. 11 for a plot of the solution.

6. Regularized Wave Equation

An important point in the preceding discussion of the wave equation is the degeneracy at $\mathscr{I}$, which is a consequence of the conformal approach. This degeneracy provided us with a particular first order boundary condition to be imposed at $\mathscr{I}$. As an alternative to the numerical solution of this *singular* equation, we investigate in this section a *regularized* version. The motivation behind this study is our future goal of solving the Einstein equations numerically on a conformally compactified space-time. Note that a regular formulation of Einstein's equations can be identified (Friedrich's regular conformal field equations, [9]).

For the derivation of the regularized wave equation, consider two conformally related n-dimensional metrics g and $\bar{g}$ with

$$\bar{g}_{\mu\nu} = \Omega^2 g_{\mu\nu}, \tag{6.1}$$

where $\Omega = \Omega(x^\mu)$ is a conformal factor. Then, the relation

$$\left(\bar{\Box} - \frac{n-2}{4(n-1)}\bar{R}\right)\left(\Omega^{1-\frac{n}{2}} f\right) = \Omega^{-1-\frac{n}{2}}\left(\Box - \frac{n-2}{4(n-1)}R\right) f \tag{6.2}$$

holds, see [16]. $\bar{R}$ and R denote the Ricci scalars of the two conformal metrics, and $\bar{\Box}$ and $\Box$ are the wave operators.[h] In our case we choose $\Omega = PQ$ [cf. (2.6)]. With $n = 4$, $R = 0$ (flat Minkowski space-time), $\bar{R} = 6$, and with the definition $\bar{f} := \Omega^{-1} f$ we obtain

$$\Box f = \Box(\Omega \bar{f}) = \Omega^3(\bar{\Box} - 1)\bar{f}. \tag{6.3}$$

[h]The wave operators are defined by $\bar{\Box} = \bar{g}^{\mu\nu}\bar{\nabla}_\mu\bar{\nabla}_\nu$ and $\Box = g^{\mu\nu}\nabla_\mu\nabla_\nu$.

Hence, equivalently to the singular equation $\Box f = 0$, we may study the regular equation

$$(\bar{\Box} - 1)\bar{f} \equiv \frac{1}{4}(\bar{f}_{,RR} - \bar{f}_{,TT}) + \frac{\bar{f}_{,R}}{\tan(2R)} - \bar{f} = 0. \tag{6.4}$$

This equation does *not* reduce to a first order boundary condition at $\mathscr{I}^+$. For the completeness of the algebraic system discussed in Sec. 3.4, we therefore need to require the nonlinear second order wave equation as a condition there. (This second order boundary condition can be imposed since no "information from outside" can encounter the numerical domain, i.e. no ingoing characteristic crosses the boundary in question.)

Again we study an explicit example by looking at the hyperboloidal IBVP (C) in Table 1, but this time we solve the *regular* wave equation (6.4). It turns out that this formulation of the problem also permits highly accurate numerical solutions. However, instead of 12 correct numerical digits (as in Fig. 6(C)), we obtain 11 digits, thereby loosing one order in the numerical accuracy.

Note that $\bar{f}$ possesses a similar accuracy as the normal derivative $\partial f/\partial n$ with respect to ingoing characteristics. In particular, the content of outgoing radiation at $\mathscr{I}^+$, described by

$$\bar{f}|_{\mathscr{I}^+} = \lim_{\Omega\to 0} \frac{f}{\Omega} \propto \left.\frac{\partial f}{\partial n}\right|_{\mathscr{I}^+}, \tag{6.5}$$

is similarly precisely given by $\bar{f}$ (calculated from the regularized wave equation) and by $\partial f/\partial n$ (calculated from the singular wave equation).

We conclude that, remarkably, our spectral algorithm is applicable to both regular and degenerate wave equations. For the fully spectral scheme, the particular formulation of a given equation seems to play a subordinate role.

7. Discussion

In this paper, we constructed numerical solutions of hyperbolic equations utilizing a fully pseudospectral scheme. Combining this method with the concept of conformal infinity, we were able to obtain highly accurate solutions.

Interestingly, by means of the method presented, hyperbolic equations can be handled quite similarly to elliptic equations. There is no principal difference between the treatment of the spatial coordinate σ and that of the time coordinate τ in the Chebyshev approximation (3.8).

The formulation of boundary/initial values is, however, fundamentally different for elliptic and hyperbolic problems. In an elliptic problem, at each boundary *one* first order condition is required, i.e. a condition which contains no second order normal derivative with respect to the boundary in question. On the other hand, a hyperbolic problem requires knowledge of the unknown function and its normal (time-) derivative at the initial slice, i.e. *two* first order conditions there. The future boundary $T = T_{\max}$ is treated like an interior point, i.e. the hyperbolic equation

provides a second order condition there. Note that any attempt to impose a first order condition at this boundary must fail[i] — not only for our pseudospectral algorithm but for any numerical scheme.

The method being presented possesses a highly implicit character. The time evolution is not performed successively, moving from one time slice to the next, but the entire system is solved simultaneously instead. As a consequence, it turned out that for all our numerical examples it was not necessary to respect a Courant–Friedrichs–Lewy (CFL) condition. In fact, the spatial collocation points could be distributed much more densely than the time points.

We have demonstrated that for solutions which admit a rapidly converging Chebyshev expansion, the method leads to an accuracy of up to 12 or 13 correct digits (for a double precision code). In all examples being discussed, the numerical error (R_{num}) is close to the analytical error (R_{an}), i.e. the algorithm proves to be very effective. Furthermore, a geometric convergence rate is exhibited, i.e. the error decreases exponentially with the resolution.

Our results encourage us to attempt to develop similar numerical techniques to solve the dynamical Einstein equations. As an interesting area of application, we envision time evolution problems of perturbed axisymmetric equilibrium configurations (as e.g. rotating stars, rings or black holes with surrounding matter). Consequently, the method would permit a highly accurate stability analysis of such objects and a careful investigation of the emitted gravitational waves at $\mathscr{I}$.

In order to apply our pseudospectral scheme to such problems, it will be necessary to cover the space-time with more than a single computational domain. (At least separate domains for matter and vacuum regions are required.) For the treatment of non-spherically symmetric equations (i.e. higher-dimensional problems), the computationally expensive direct matrix inversion in the Newton Raphson method needs to be replaced by an iterative inversion method, as already mentioned earlier. We believe that through the implementation of appropriate technical details our method becomes applicable to the solution of such physically interesting problems.

Acknowledgments

We would like to thank Helmut Friedrich, Jérôme Novak, Silvano Bonazzola, and David Petroff for many valuable discussions. This work was supported by the Deutsche Forschungsgemeinschaft (DFG) through the Collaborative Research Centre SFB/TR7 “Gravitational wave astronomy”.

Appendix A. Plots of the Example Solutions

Within this appendix, we provide plots of all numerical example solutions to the linear, inhomogeneous and non-linear wave equation that we have studied in this paper.

[i] As an example, for the wave equation a particular Dirichlet type boundary value problem can be shown to admit infinitely many solutions.

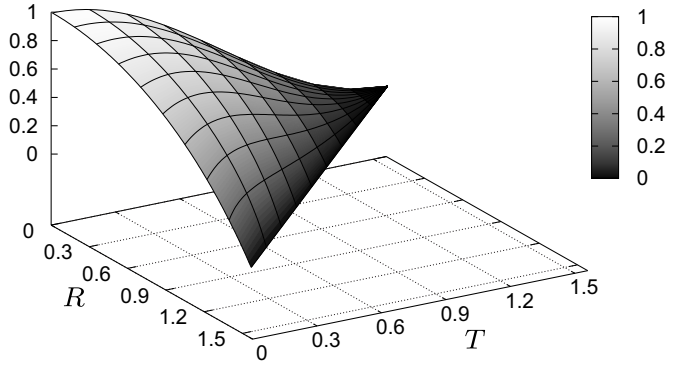

Fig. 9. Solution to the linear wave equation with $A(x) = x$, cf. Figs. 4 and 5.

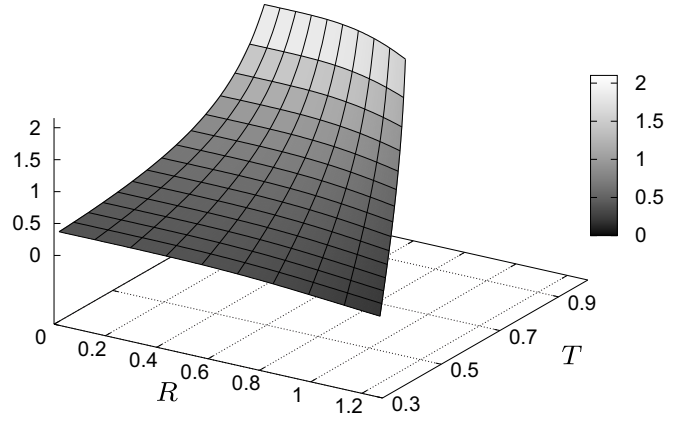

Fig. 10. Example solution to the inhomogeneous wave equation, cf. Fig. 7.

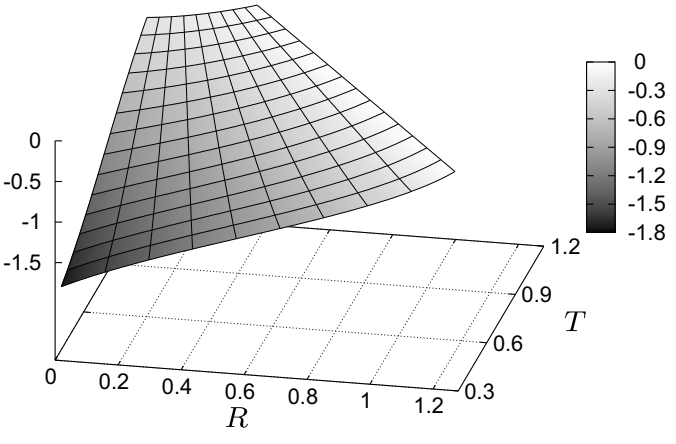

Fig. 11. Example solution to the non-linear wave equation, cf. Fig. 8.

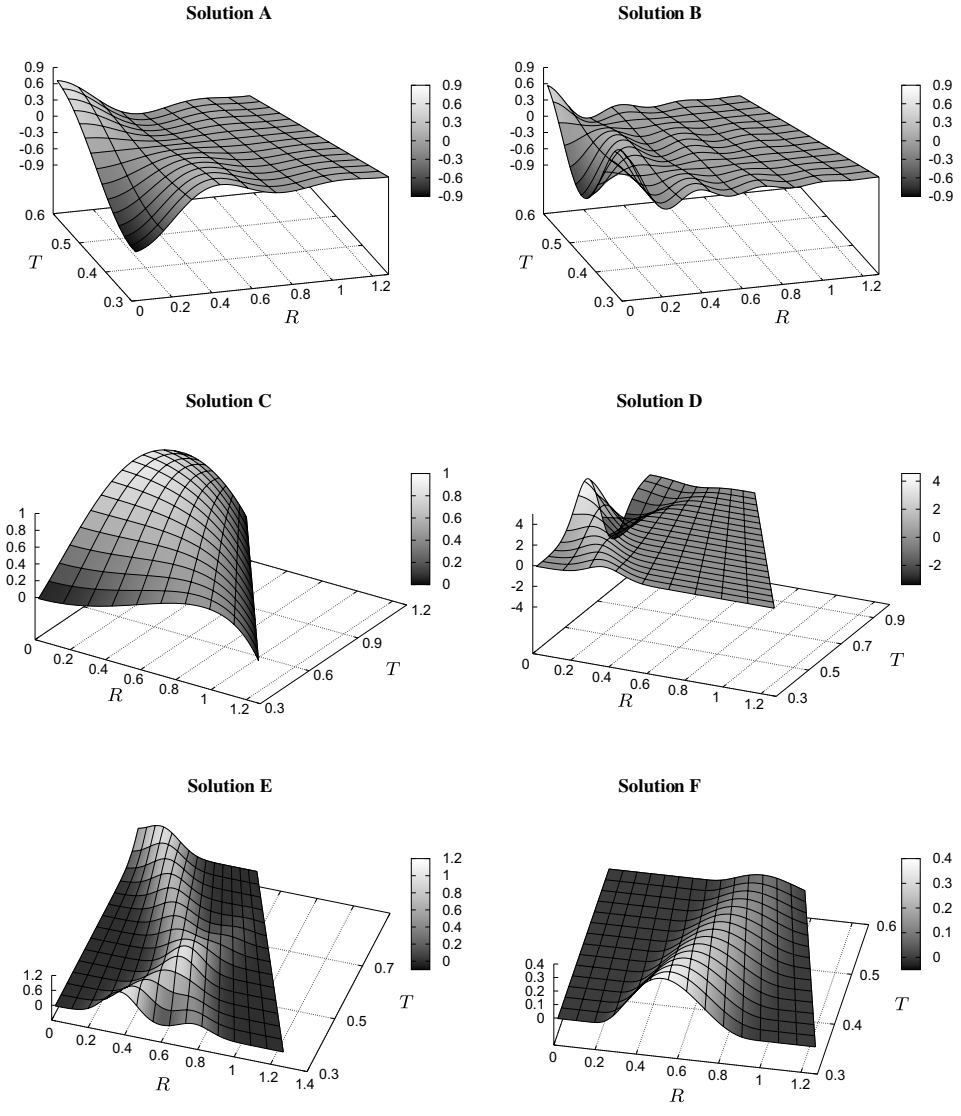

Fig. 12. Numerical examples for the hyperboloidal IBVP of the linear wave equation in Table 1, cf. Fig. 6.

References

[1] L. Andersson, P. T. Cruściel and H. Friedrich, On the regularity of solutions to the Yamabe equation and the existence of smooth hyperboloidal initial data for Einstein's field equations, *Commun. Math. Phys.* **149** (1992) 587–612.

[2] L. Andersson and P. T. Cruściel, On hyperboloidal Cauchy data for vacuum Einstein equations and obstructions to smoothness of scri, *Commun. Math. Phys.* **161** (1994) 533–568.

[3] M. Ansorg, A. Kleinwächter and R. Meinel, Highly accurate calculation of rotating neutron stars, *Astron. Astrophys.* **381** (2002) L49–L52.
[4] M. Boyle, D. A. Brown, L. E. Kidder, A. H. Mroue, H. P. Pfeiffer, M. A. Scheel, G. B. Cook and S. A. Teukolsky, High-accuracy comparison of numerical relativity simulations with post-Newtonian expansions, *Phys. Rev. D* **76** (2007) 124038.
[5] J. Corvino, Scalar curvature deformation and a gluing construction for the Einstein constraint equations, *Commun. Math. Phys.* **214** (2000) 137–189.
[6] S. Dain and H. Friedrich, Asymptotically flat initial data with prescribed regularity at infinity, *Commun. Math. Phys.* **222** (2001) 569–609.
[7] J. Frauendiener, Conformal infinity, *Living Rev. Relativity* **7** (2004) 1, URL: cited on 29 November 2007, http://www.livingreviews.org/lrr-2004-1.
[8] J. Frauendiener, Calculating initial data for the conformal field equations by pseudospectral methods, *J. Comput. Appl. Math.* **109** (1999) 457–491.
[9] H. Friedrich, Conformal Einstein evolution, in *The Conformal Structure of Space-Time* (Springer-Verlag, Berlin, Heidelberg, New York, 2002), pp. 1–50.
[10] P. Grandclément and J. Novak, Spectral methods for numerical relativity, *Living Rev. Relativity* **12** (2009). URL: cited on 18 February, 2009, http://www.livingreviews.org/lrr-2009-1.
[11] P. Hübner, A scheme to numerically evolve data for the conformal Einstein equation, *Class. Quant. Grav.* **16** (1999) 2823–2843.
[12] S. Husa, Numerical relativity with the conformal field equations, in *Proceedings of the Spanish Relativity Meeting*, Madrid (2001), Lecture Notes in Physics (Springer-Verlag, Heidelberg, Germany, 2002).
[13] G. Ierley, B. Spencer and R. Worthing, Spectral methods in time for a class of parabolic partial differential equations, *J. Comput. Phys.* (1992) 88–97.
[14] R. Penrose, The light cone at infinity, in *Relativistic Theories of Gravitation* (Pergamon Press, Oxford, 1964), pp. 369–373.
[15] A. Üngör, A. Sheffer, R. B. Haber and S.-H. Teng, Layer based solutions for constrained space-time meshing, *Appl. Numer. Math.* **46** (2003) 425–443.
[16] R. M. Wald, *General Relativity* (University of Chicago Press, Chicago, 1984).
[17] A. Zenginoğlu, A conformal approach to numerical calculations of asymptotically flat spacetimes, Ph.D. thesis, Max Planck Institute for Gravitational Physics and University of Potsdam, Germany (2007), gr-qc/0711.0873.